Analyst

Accepted Manuscript

ROYAL SOCIETY OF CHEMISTRY

www.rsc.org/analyst

Graphical Abstract

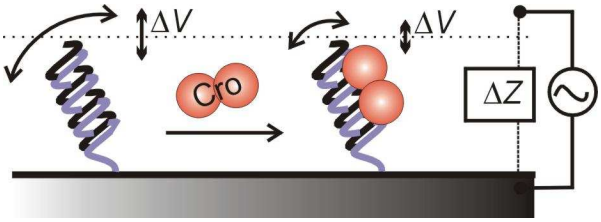

Changes in diffusive movements, surface potential, and interfacial impedance of DNA monolayers are combined to analyze binding of unlabeled transcription factors.

Multimodal Electrochemical Sensing of Transcription Factor-Operator Complexes

*Keeshan Williams, Chung-Sei Kim, Jin Ryoun Kim and Rastislav Levicky**

Department of Chemical & Biomolecular Engineering, Polytechnic Institute of New York University, Brooklyn, New York 11201

AUTHOR EMAIL ADDRESS: rl1306@nyu.edu

Graphical Abstract

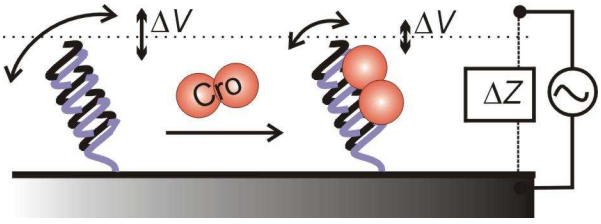

Changes in diffusive movements, surface potential, and interfacial impedance of DNA monolayers are combined to analyze binding of unlabeled transcription factors.

Abstract. Interactions of proteins with nucleic acids arise at all levels of cellular function, from chromosomal packing to biological regulation. These interactions can be analyzed in a high-throughput fashion by immobilizing the DNA sequences of interest, possibly numbering in the thousands, at discrete locations on a solid support and identifying those sequences that a protein analyte binds. Ideally, such surface assays would use unlabeled analyte to simplify protocols and avoid the possibility of perturbing the protein/DNA interaction. The present study compares three electrochemical modalities for simultaneously detecting binding of unlabeled transcription factor proteins to immobilized DNA duplexes based on (i) changes in the duplex diffusive motions, (ii) variations in the surface potential, and (iii) variations in the interfacial charging impedance, all of which can be conveniently derived from AC voltammetry traces. Cro protein from bacteriophage lambda is used as a model transcription factor. Specific binding of protein was successfully detected through modalities (i) and (ii), but not (iii). The effectiveness of these techniques is compared as a function of sampling frequency and protein concentration. Binding of 15 kDa Cro slowed down rotational diffusion of immobilized duplexes approximately 3-fold, and induced up to 5 mV changes in the surface potential. Moreover, by assessing Cro binding to bacteriophage operators of variable affinity, the study illustrates how contrast between specific and nonspecific interactions impacts detection.

1. Introduction

Interactions between proteins and nucleic acids serve functions ranging from gene expression to DNA replication, repair, and packaging. The need for convenient and scalable analysis of these interactions motivated, over the past decade, development of solid-phase alternatives to traditional immunoprecipitation[1] and electrophoretic methods.[2] Solid-phase approaches have been used to quantify proteins in crude cellular extracts,[3] to establish sequence context of DNA/protein interactions at genomic scales,[4–6] and to study fundamental mechanisms of protein redox-activity and enzymatic DNA repair.[7–9] Examples include protein binding microarrays (PBMs), in which protein binding is examined following a wash step with detection typically realized through fluorescence immuno-staining for the assayed protein.[6] Although PBMs do not provide real-time data, real-time operation, needed for kinetic and robust thermodynamic analysis, is possible with total internal reflection fluorescence (TIRF) analysis.[4] A strength of fluorescence-based methods is capability for multi-dye approaches; e.g. to confirm composition of protein complexes[4] or to co-localize DNA and bound protein.[10] Electrochemical techniques can provide additional information not accessible with optical and fluorescence methods. For example studies of DNA-mediated charge transport have elucidated mechanisms behind binding-induced redox activity of proteins containing iron-sulfur clusters,[7,8,11] and detected DNA conformational changes in response to association with transcription factors.[12]

Characterization techniques based on contrast mechanisms arising from native molecular properties are especially convenient in that they do not require modification of the analyte, yet provide general means for monitoring biomolecular associations. DNA/protein interactions have been followed optically using surface plasmon resonance methods,[13–15] which exploit changes in refractive index that accompany protein complexation with DNA on a solid support.

DNA/protein associations have been also monitored electrochemically by detecting protein binding through perturbation in electron transfer rates from electroactive tags covalently bound to the nucleic acid.[3,16–18] The electron transfer reflects changes in DNA conformation and diffusive motions induced by protein binding, and can be characterized with techniques such as cyclic voltammetry,[19] alternating current voltammetry (ACV),[17] or square wave voltammetry.[20]

The present study demonstrates simultaneous application of multiple "reagent-free" electrochemical modalities for tracking binding of unlabeled proteins to immobilized DNA operators. Use of multiple transduction mechanisms based on different physical contrasts can expand the spectrum of detectable analytes and improve reliability of detection. Three methods are used to monitor DNA monolayers undergoing complexation with a transcription factor protein. The three modalities, although derived from a single AC voltammetry experiment, track different physical phenomena including the DNA diffusive motions, the potential difference between the sensing surface and solution,[21,22] and the nonfaradaic interfacial impedance. In addition, by choosing the Cro transcription factor from bacteriophage lambda and its three operator sites in the P_{RM}/P_R promoter region,[23–25] the operator-specific binding affinity can be varied by about two decades,[26,27] a feature convenient for examining how interplay between specific and nonspecific binding impacts detection of the desired, specific interactions.

2. Experimental Methods

2.1. Reagents. Monobasic and dibasic sodium phosphate (Spectrum Chemicals), sodium carbonate (Fisher), sodium bicarbonate (Fisher), 6-mercapto-1-hexanol (MCH; Sigma Aldrich), acetonitrile (ACN; Spectrum Chemicals), dimethyl sulfoxide (DMSO; Sigma Aldrich), sulfuric acid (H_2SO_4; Fisher), potassium chloride (KCl; Acros Organics), triethylammonium acetate

(TEAA; Glenn Research), and *N*-succinimidyl ferrocenecarboxylate (FcCA-NHS; TCI America) were reagent grade from the respective providers and used as received. Aqueous solutions were prepared with deionized 18 MΩ cm resistivity water from a Milli-Q water purification system.

2.2. Protein Expression and Purification. Bacteriophage λ Cro protein was expressed following a literature protocol.[28] A commercially available plasmid vector, pGS-21a containing the DNA sequence of Cro (Genescript Corporation), was used to transform *Escherichia coli* strain BL21. Cell growth, overexpression of Cro, cell harvesting, and isolation of low molecular weight proteins were conducted in close observance of Hall *et.* al.[28] Fast protein liquid chromatography purification of Cro was performed by loading the low molecular weight protein products onto a HiTrap Q (GE Healthcare) anion exchange column equilibrated with PC buffer (20 mmol L^{-1} Tris pH 8.0, 0.1 mmol L^{-1} EDTA, 5 % glycerol, and 1.4 mmol L^{-1} *β*-mercaptoethanol), where fractions of the positively charged Cro were collected in the flow through. These were concentrated and loaded onto a HiTrap HP (GE Healthcare) cation exchange column equilibrated with PC buffer, followed by elution on a gradient of PC buffer and 1 mol L^{-1} NaCl. Fractions matching the molecular weight of Cro were identified using SDS-PAGE electrophoresis on 4-12 % NuPAGE bis-tris precast gels with Mark 12 protein standard (Invitrogen). Purity of protein was qualitatively confirmed by observing alignment between the dominant gel band and the appropriate band on the protein standard. Positively identified Cro fractions were concentrated and loaded onto a HiPrep 26/10 desalting column (GE Healthcare) equilibrated with deionized water. Fractions were collected once more, concentrated, lyophilized, and stored at -80 °C. Protein identity was verified using matrix-assisted laser desorption/ionization time of flight mass spectrometry (MALDI-TOF MS), with unique amino acid fragments obtained from proteolytic digestion with trypsin confirmed by comparison to the

expected digestion pattern. Cro concentrations were determined using a Bradford assay[29,30] with bovine serum albumin (BSA) as the calibration standard.

2.3. DNA Sequences. Binding of Cro was studied to four different duplex sequences: three from the lambda genome carrying the 17-bp long OR_1, OR_2, and OR_3 operator sites, and the fourth a nonspecific control to which Cro was not expected to bind. Table 1 lists the sequences used, with bold letters highlighting the operator sites. Duplexes were immobilized to gold electrodes through the 5' ends of "probe" strands, which included extra thymine residues as spacers and a chemisorbing disulfide moiety. Terminal 3' amine groups were used for modification with electroactive ferrocene labels. All oligonucleotides were obtained with standard desalting (Integrated DNA Technologies).

Table 1. DNA Sequences (operator sites are bold faced).

Duplex	Type[a]	DNA sequence (including end modifications)
OR_1	Probe	5'-HO-$(CH_2)_6$-S-S-$(CH_2)_6$-TTTTT**TATCACCGCCAGAGGTA**AT-NH_2-3'
	Target	5' -AT**TACCTCTGGCGGTGATA**AA-NH_2-3'
OR_2	Probe	5'-HO-$(CH_2)_6$-S-S-$(CH_2)_6$-TTTTC**TAACACCGTGCGTGTTG**AC-NH_2-3'
	Target	5'-GT**CAACACGCACGGTGTTA**GA-NH_2-3'
OR_3	Probe	5'-HO-$(CH_2)_6$-S-S-$(CH_2)_6$-TTTTC**TATCACCGCAAGGGATA**AA-NH_2-3'
	Target	5'-TT**TATCCCTTGCGGTGATA**GA-NH_2-3'
NS	Probe	5'-HO-$(CH_2)_6$-S-S-$(CH_2)_6$-TTTGAGCGAGTATTGCTTGCAGGG-NH_2-3'
	Target	5'-CCCTGCAAGCAATACTCGCTC-NH_2-3'

[a] Each duplex consisted of a "probe" and a complementary "target" strand, with immobilization through the probe strand.

For electrochemical measurements, probe strands were labeled at their amino termini with FcCA-NHS.[31] Labeling proceeded by combining DNA and FcCA-NHS in a ratio of 150 μmol L^{-1} to 25 mmol L^{-1}, respectively, in a solution of 21 % DMSO and 79 % 0.4 mol L^{-1} sodium carbonate buffer at pH 9. The reaction proceeded for 15 h at 37 °C with gentle shaking. The DNA-FcCA conjugates were desalted on NAP-10 columns (GE Healthcare) with deionized

water as the equilibrium and elution buffer, followed by purification with reverse phase HPLC using a 0.1 mol L^{-1} pH 7 TEAA / ACN gradient.

2.4. Derivatization of Working Electrodes. Solutions of DNA-FcCA probes and unlabeled complementary targets were combined in a ratio of 1 to 1.5 at a total strand concentration of 0.3 μmol L^{-1} in 200 μL of 0.2 mol L^{-1} pH 7 sodium phosphate buffer. To facilitate formation of equilibrated duplex structures, the solutions were subjected to three cycles of thermal denaturation at 85 °C for 10 min followed by annealing at 25 °C for 10 min using a thermal cycler with a temperature ramp of 3 °C s^{-1} (Mastercycler gradient, Eppendorf). 1.6 mm diameter gold working electrodes (Bioanalytical Systems) were mechanically polished with 1 μm diamond polish (Bioanalytical Systems), followed by two rounds of 2 min sonication in methanol and 2 min sonication in water. Next, two rounds of electrochemical polishing were performed with cyclic voltammetry (CV). Each round consisted of two sets of 20 CV cycles in 10 mmol L^{-1} KCl / 0.5 mol L^{-1} H_2SO_4, with immersion in fresh solution each time, followed by two such sets in 0.5 mol L^{-1} H_2SO_4. CVs were performed between -0.2 and 1.7 V using a 0.5 V s^{-1} scan rate. All electrode potentials are expressed relative to an Ag/AgCl/sat KCl reference electrode. After polishing, working electrodes were washed in deionized water and surface roughness factors *r*, with *r* the ratio of total to geometric electrode area, were measured as described.[32,33] After a final water rinse, electrodes were immersed in the 0.3 μmol L^{-1} solution of probe/target duplexes at room temperature for 15 min while maintaining a 0 V bias. At the end of the 15 minutes, a blocking step was performed for 5 min in 0.1 mmol L^{-1} solution of MCH in deionized water under the same conditions.[34] Surface blocking introduces hydroxyl groups to the electrode so as to suppress nonspecific adsorption of the DNA.[34,35]

2.5. Electrochemical Measurements. All measurements were performed in 0.2 mol L^{-1} pH 6 sodium phosphate buffer, hereafter referred to as "SPB", at approximately 25 ^{o}C. Surface blocking agents such as bovine serum albumin (BSA) were not used as these could also adsorb to the working electrode;[36,37] on the other hand, this raised the risk of Cro losses due to nonspecific adsorption on labware. AC voltammetry (ACV) data were collected with amplitude of 10 mV and modulation frequencies of 1, 6, 10, 30, 50, 100, 250, 750, 1000, 5000 and 10000 Hz, over a potential window from 0 to 0.7 V. Data were analyzed in three ways: (i) for dynamics of duplex rotational reorientation based on the magnitude of ferrocene current, interpreted to reflect the number of duplex FcCA tags that diffuse sufficiently close to the electrode to participate in electron transfer within a sampling interval; (ii) for the formal potential of the FcCA tags, interpreted to reflect changes in energetics of FcCA electroactivity due to altered composition of their surroundings; and (iii) for changes in the in- and out-of-phase impedances of the nonfaradaic (i.e. charging) portion of the ACV signal, interpreted to reflect variations in the polarizability, ionic screening, and/or conductivity at the electrode surface. All measurements were performed on a three-electrode setup that included the DNA-modified gold working electrode, a platinum counter electrode, and an Ag/AgCl/sat KCl reference, connected to a CH Instruments 1040A 8-channel multi-potentiostat. As the diffusive motions of DNA duplexes are affected by their surface coverage,[38,39] experiments were conducted at relatively low coverages of 3×10^{11} to 6×10^{11} chains cm^{-2}. Duplexes were not expected to interact strongly at these coverages since their average separation exceeded 14 nm, compared to their length of about 8 nm.

Protein titration was performed over nearly four decades in Cro concentration, from 6×10^{-10} to 2×10^{-6} mol L^{-1}. ACV voltammograms were collected 30 min after addition of each new concentration, with stirring.

2.6 Data Analysis. Experimental ACV traces were fit to equation 1[40]

$$I_{avg}(E_{dc}) = mE_{dc} + b + \left[(2nfFN_{app}) \frac{\sinh(\frac{nFE_{ac}}{RT})}{\cosh(\frac{nFE_{ac}}{RT}) + \cosh\left[(\frac{nF}{RT})(E_{dc} - E_0)\right]} \right] \quad (1)$$

where I_{avg} is the average AC current when the electrode potential is cycled with frequency f and amplitude E_{ac} at a DC bias E_{dc}, m and b are the slope and intercept of the baseline correction, n is the number of electrons involved in the redox event (n = 1 for FcCA), F is Faraday's constant, E_0 is the FcCA formal potential, R is the gas constant, and T is absolute temperature. In the absence of limitations on electron transfer N_{app} in equation 1 would equal the total number of redox tags on the immobilized DNA. This situation is approximated at low sampling frequencies f for which all duplexes have time to re-orient so as to bring their FcCA tags close to the electrode; thus, electron transfer is not rate limited. At higher frequencies, only a fraction of tags will contribute to the measured ACV current and N_{app} becomes an effective, f-dependent quantity whose value is constrained by any rate limitations on charge transport that persist over timescales longer than ~ 1/f. N_{app}, in moles, can be converted to an apparent duplex coverage $S_{D,app}$

$$S_{D,app} = \frac{N_{app} N_A}{r A_g} \quad (2)$$

where N_A is Avogadro's number, A_g is the geometric area of the working electrode (0.020 cm^2), and r is the measured roughness factor. Equation 1 was fit to experimental data by varying m, b, N_{app}, and E_0 using the lsqcurvefit function in Matlab, which performs a least squares

minimization on the residuals between experimental and fitted values. Figure 1 illustrates the frequency dependence of $S_{D,app}$.

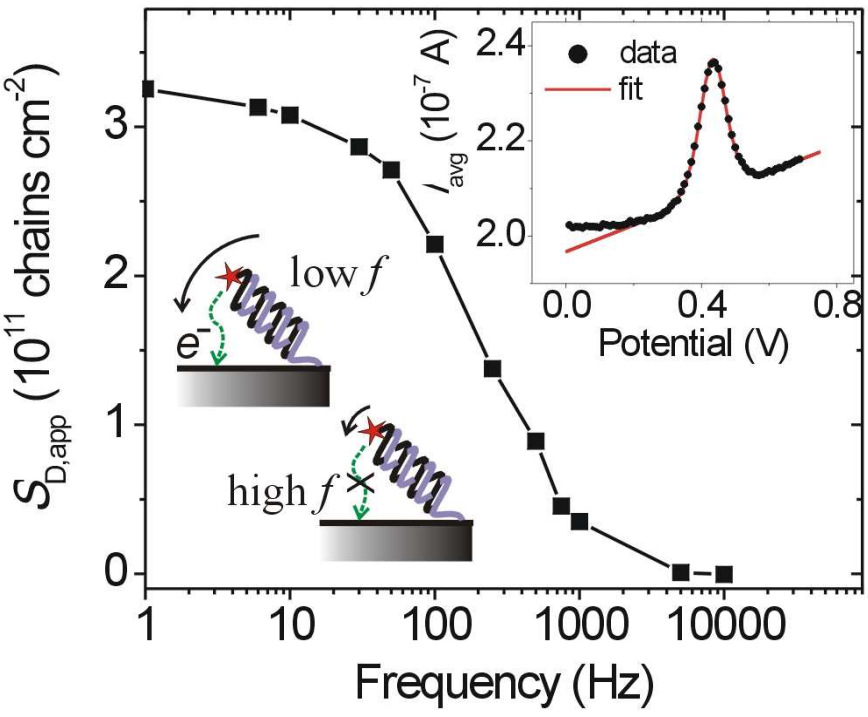

Figure 1. Dependence of $S_{D,app}$ on ACV sampling frequency for a monolayer of distally labeled (inset, bottom left) DNA duplexes. The top right inset shows ACV data for the point at 100 Hz, including a fit to equation 1 from which N_{app} was estimated.

ACV data were also analyzed for the formal potential E_0 of FcCA, and for the impedance Z. E_0 was obtained during fitting of equation 1 at frequencies below 1000 Hz; for higher frequencies the FcCA peak was too small to estimate E_0. The real Z' and imaginary Z'' components of impedance were calculated from

$$Z' = \frac{V_{ac} I_{ip}}{(I_{ip}^2 + I_{op}^2)} \qquad Z'' = -\frac{V_{ac} I_{op}}{(I_{ip}^2 + I_{op}^2)} \qquad (3)$$

where V_{ac} is the magnitude of the imposed AC potential, and I_{ip} and I_{op} are the measured in- and out-of-phase current components, respectively. Whereas N_{app} and E_0 were calculated from the faradaic response of the FcCA tags, Z' and Z'' were averages derived from data for potentials between 0 and 0.1 V, which fall below onset of significant FcCA activity.

Because ferrocene is susceptible to breakdown in its oxidized ferricenium form,[31,41,42] several precautions were taken. Dissolved oxygen, which promotes ferrocene oxidation, was reduced by degassing of solutions prior to experiments and blanketing with nitrogen during experiments. Second, oxidation of ferrocene tags during data collection was minimized by keeping the ACV sampling period fairly short (~ 0.2 s). Third, $^{-}$OH mediated degradation of ferrocenium[43] was decreased by using a slightly acidic buffer of pH 6. Lastly, data were normalized to compensate for any remnant degradation. Because low frequencies allow nearly all active tags on the electrode to undergo electron transfer, the low frequency limit was used to track loss of tag activity. This normalization was performed for each frequency by dividing the N_{app} value by its low frequency limit, $\bar{N}_{low}$, as averaged over the three lowest frequencies of 1, 6, and 10 Hz.

3. Results and Discussion

3.1. Data Overview. Use of linear DNA duplexes raised the possibility that duplexes would dehybridize, since only one strand of each duplex was immobilized. Alternately, internally-hybridized duplex structures, such as DNA hairpins,[16] could be also used; however, it was desirable to stay as close as possible to native linear organization of DNA. Stability of DNA duplexes was assessed through repeated rounds of Cro addition followed by removal of bound

protein through denaturation with sodium dodecyl sulfate (SDS), Figure 2. Measurements were obtained at 100 Hz by alternately immersing an OR_3 duplex monolayer in fresh solutions of SPB with 2.1 × 10^{-7} mol L^{-1} Cro ("Cro On" stages), followed by immersion in SPB with 0.5 % w/v SDS ("Cro Off" stages). The similar changes in magnitude between "Cro Off" and "Cro On" stages indicate that DNA duplexes did not significantly dehybridize over the 8 h experimental durations of interest. If instead target strands had desorbed they would have left single-stranded probes that would not bind Cro, so that the change in signal between stages would be suppressed. The gradual downward drift in overall intensity is attributed to tag degradation, which was not calibrated for in Figure 2 in order to illustrate magnitude of this effect.

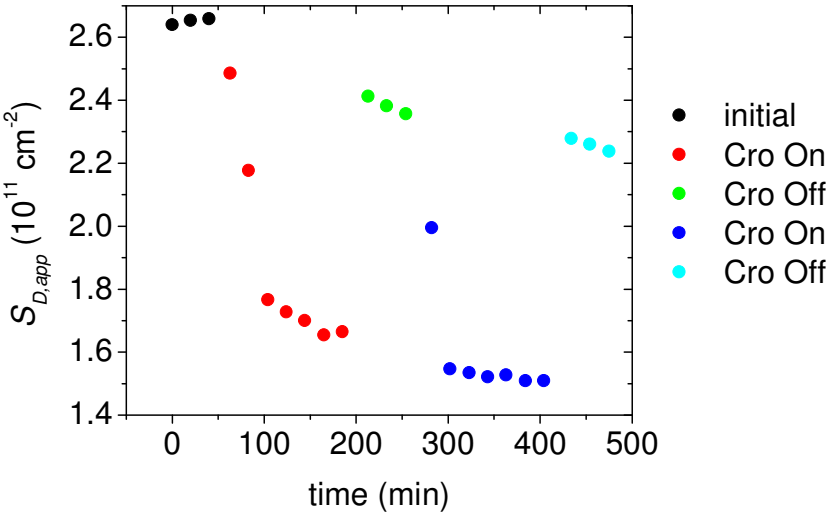

Figure 2. $S_{D,app}$ derived under initial conditions without Cro (3 scans), followed by two cycles of Cro addition (7 scans) and its removal by denaturation with SDS (3 scans). Data points were taken every 20 min at 100 Hz using OR_3-DNA duplexes in SPB. Cro concentration: 2.1 x 10^{-7} mol L^{-1}.

Binding assays were performed with electrodes of all four duplexes (OR_1, OR_2, OR_3 and NS) immersed together in the same series of Cro solutions. The concentration of protein on a Cro monomer basis, C_P, was gradually increased from 6×10^{-10} to 2×10^{-6} mol L^{-1} by titrating in protein. At each value of C_P a full frequency sweep was performed from 1 to 10,000 Hz. Figures 3A and 3B show the complete results for the highest (OR_3) and weakest (NS) affinity operators, while Figure 3C plots frequency-averaged responses for all four operators. Frequency averaging was performed from 10 to 250 Hz for the N_{app} and from 1 to 1000 Hz for the E_0 modality, representing ranges in f for which these modalities were sensitive to Cro binding (cf. section 3.2). Figure 4 plots examples of impedance data, presented as the magnitude $Z = (Z'^2 + Z''^2)^{1/2}$ and phase angle $\theta = \text{atan}(Z''/Z')$. In contrast to N_{app} and E_0, impedance did not provide clear distinction between specific and nonspecific binding.

Perhaps surprisingly, onset of Cro binding occurred at fairly similar C_P for all three operators (Fig. 3C), despite the thermodynamic expectation that the highest affinity OR_3 should respond at nearly two decades lower concentration than the weakest affinity OR_2[26] (the actual onset for OR_3 was at a 3-fold lower Cro concentration than for OR_2). This observation is attributed to mass transport limitations at low concentrations preventing sufficient accumulation of Cro during the 30 min measurement interval between successive concentrations. Mass transport limitations are further exacerbated by need for Cro dimers, which only represent a small fraction of total Cro at these low concentrations; e.g. about 0.3 % of total Cro at C_P of 1×10^{-9} mol L^{-1} and 3 % at C_P of 1×10^{-8} mol L^{-1}.[44] These conditions translate to dimer concentrations well below nanomolar, requiring hours to reach equilibrium. Measurements (cf. Figure 2) indicate that saturation requires 30 to 60 min for C_P near 1×10^{-7} mol L^{-1}, in agreement with onset of significant binding at around this concentration in Figure 3C.

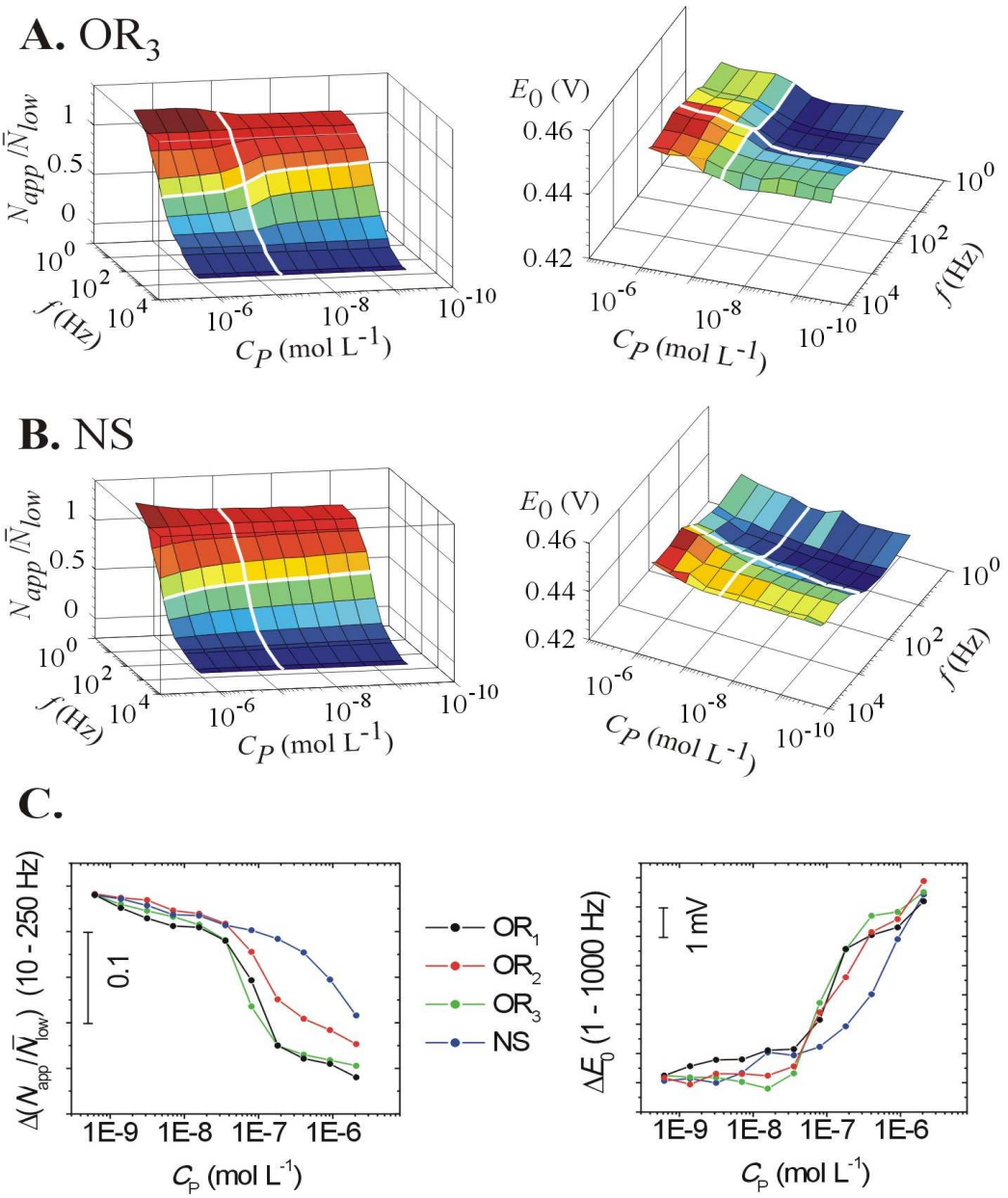

Figure 3. Cro binding maps as a function of ACV frequency f and Cro concentration C_P, performed in triplicate and averaged. ACV data were analyzed as described in section 2.6 to derive $N_{app}/\bar{N}_{low}$ and E_0. Data for **(A)** OR_3 and **(B)** NS duplexes at surface coverages of 4.9 ± 0.7 x 10^{11} and 4.3 ± 0.8 x 10^{11} duplexes cm^{-2}, respectively. Thicker white lines mark conditions corresponding to f = 100 Hz and $C_P = 8 \times 10^{-8}$ mol L^{-1}. **(C)** Titration curves in the N_{app} and E_0

modalities for all four duplex sequences. After averaging over the indicated range in *f*, to facilitate comparison curves were translated along the *y*-axis to align at the lowest concentration.

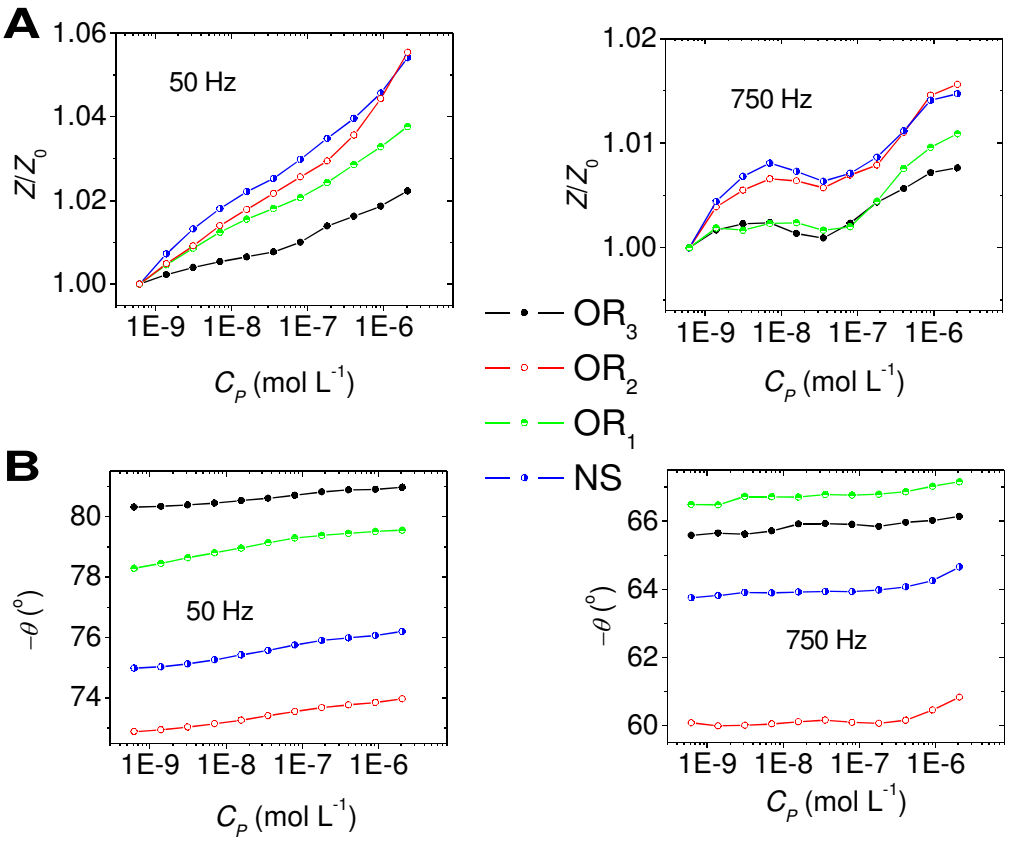

Figure 4. Nonfaradaic impedance data, presented as the **(A)** magnitude *Z* and **(B)** phase angle θ, for Cro binding to the OR_1, OR_2, OR_3, and NS duplexes. In (A), to compensate for differences in electrode area, *Z* values were normalized by the value Z_0 measured for the lowest Cro concentration of 0.62×10^{-9} mol L^{-1}. Data are plotted for two frequencies, 50 and 750 Hz, to illustrate the range of response observed toward lower and higher frequency limits.

The results in Figure 3C illustrate that specific and nonspecific interactions manifest differently in the N_{app} and E_0 responses, while they produce rather similar trends in nonfaradaic

impedance, Figure 4. Nonspecific interactions could be driven by attraction between the positively charged protein, with an estimated valency of +6 per monomer at pH 6, and the negatively charged DNA backbone, or by direct adsorption of Cro to the MCH-passivated electrode.

3.2. Diffusive Dynamics (N_{app}). Following the physical framework presented by Anne and Demaille for ferrocene-modified, immobilized duplex DNA,[45] changes in N_{app} are interpreted to reflect adjustments in the rotational diffusive motions of the tethered duplexes. These diffusive motions periodically bring each FcCA tag to/from the solid support, thus facilitating or impeding electron transfer. During potential cycling at low *f*, nearly all tags have time to approach the surface. Under these conditions N_{app} is maximized and the ratio $N_{app}/\bar{N}_{low}$ approaches unity. If the sampling frequency is increased, however, the fraction of tags undergoing electron transfer within a sampling period will decrease, thus lowering N_{app}. Binding of protein will alter the DNA diffusive motions; the factors behind such changes are expected to be both steric, where bound Cro blocks certain paths of approach for the FcCA tags to the electrode, as well as hydrodynamic where bound protein increases the drag coefficient relative to the unbound duplex. Such phenomena were first exploited for analysis of DNA-binding proteins by Plaxco and collaborators in the context of the TATA-box binding protein, thrombin, a methyltransferase, and a prokaryotic single-strand binding protein.[3,16,17]

In the λ Cro system, influence of protein binding was most pronounced for sampling frequencies of 30, 50 and 100 Hz, Figure 5. The decreased contrast at lower frequencies is attributed to duplexes being able to undergo electron transfer whether or not bound by Cro, while at higher frequencies even unbound duplexes reoriented too slow for the rate of sampling. The

shift along the *f*-axis indicates that binding of the protein decreased the rate of electron transport about 3-fold – a significant impact for the rather small, ~ 15 kDa Cro dimer.

Taking the midpoint f_{mid} of the binding response as an estimate of the diffusional reorientation time $\tau_r = 1/f_{mid}$ yields τ_r = 0.008 s and 0.027 s below and above binding, respectively. These values correspond to apparent rotational diffusion coefficients D_r in the range 10 to 100 s^{-1}, and as such are comparable to a value of 200 s^{-1} reported by Anne and Demaille in a study of immobilized 20mer duplexes.[45] As also noted by those authors, the surface D_r values are about five decades lower than expected based on unhindered rotational diffusion for duplex oligonucleotides in solution,[46] a discrepancy attributed to constraints on the rotational mobility of immobilized duplexes. Factors expected to interfere with duplex rotation include steric hindrances from tight end-immobilization against the MCH monolayer as well as the need to displace water of hydration around the DNA[47] and/or the MCH monolayer should duplexes align parallel to the support.

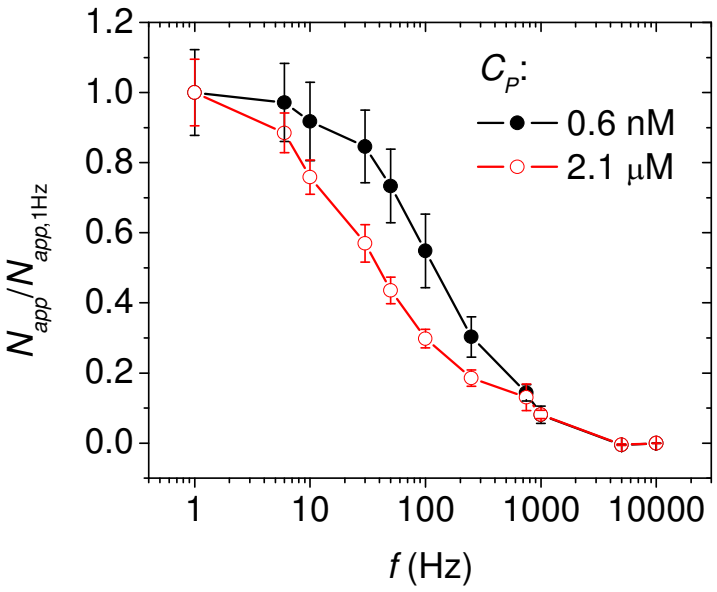

Figure 5. Frequency-dependence of N_{app}, measured for OR_3 duplexes, for Cro concentrations below (-●-) and above (-o-) occurrence of protein binding. The data correspond to slices along

the *f*-axis in Figure 3A, left. Uncertainties are standard deviations over three independent electrode preparations.

From the left panel in Figure 3C both specific (OR_1, OR_2, OR_3) and nonspecific (NS) interactions impact N_{app}. As C_P increases, specific interactions approach saturation around 1×10^{-7} mol L^{-1}, while the nonspecific response continues to gradually increase over the entire investigated range in Cro (up to 2.1×10^{-6} mol L^{-1}). Interestingly, the specific response at saturation for the weakest operator OR_2 was diminished relative to the higher affinity operators (the reported solution affinities are 6.9×10^9 L mol^{-1} for OR_3, 6.5×10^8 L mol^{-1} for OR_1, and 8.5×10^7 L mol^{-1} for OR_2 [26]). This suggests a correlation between binding affinity and impact on rotational mobility of immobilized DNA duplexes. Physical origins of such a correlation could reflect, for example, a more facile readjustment of the protein on the DNA when the underlying interactions are sufficiently weak, what could diminish the steric hindrance to DNA reorientation from a bound protein.

3.3. Surface Redox Potentials (E_0). Binding of Cro triggered a positive shift in the FcCA potential E_0, with the shift (ΔE_0) appearing at about the same Cro concentration C_P as the changes observed for N_{app}. As the two detection modalities derive from different contrast mechanisms, they provide independent confirmation of protein binding. A readily detectable ΔE_0 of up to 5 mV was observed over three decades in frequency, Figure 6. The positive displacement in E_0 can be interpreted in terms of a change in the oxidation energetics from ferrocene to ferricenium induced by protein binding. In such a mechanism, accumulation of positively-charged Cro would be expected to hinder generation of like-charged ferricenium, leading to higher potential for oxidation. Similar shifts were observed for all three λ operators, Figure 3C, indicating that perturbation of the redox energetics by Cro binding did not strongly depend on

operator sequence. Although we are not aware of E_0 shifts having been used for analysis of DNA/protein binding (but noting work on induction of protein electroactivity[7,8]), such shifts can be seen in published data on proteins other than λ Cro (e.g. see ref [16]); thus, we expect this modality to be fairly general.

The E_0 mechanism has certain advantages relative to N_{app}. These include robustness, so long as a peak can be resolved, to signal decrease for reasons other than protein association (e.g. due to probe deactivation, desorption, or tag degradation), and in the case of Cro binding a useable frequency range that is broader than for N_{app} (cf. Figures 5 and 6). On the other hand, based on Figure 3C, E_0 appears less effective in separating specific from nonspecific contributions since impact from nonspecifically-associating protein became significant at a lower protein concentration for E_0 than for N_{app}. The reasons why nonspecifically-bound protein would impact tag oxidation somewhat differently from its effect on diffusive movements of the immobilized duplexes remain to be determined.

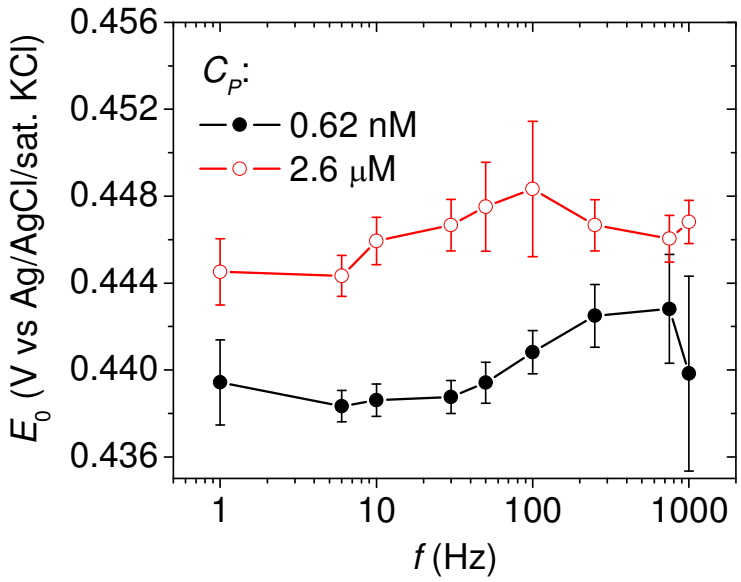

Figure 6. Frequency-dependence of E_0, measured for OR_3 duplexes, for Cro concentrations below (-●-) and above (-o-) occurrence of protein binding. The data correspond to slices along

the *f*-axis in Figure 3A, right. Uncertainties are standard deviations over three independent electrode preparations. Due to gradual disappearance of ACV peaks at higher frequencies, E_0 values are less reliable in this limit.

The absolute magnitude of E_0 tended to decrease for lower frequencies, Figure 6, whether or not protein was bound. A decrease in E_0 at lower frequencies indicates that contributions from more readily oxidized tags increased in this limit; that is, that more readily oxidized tags had slower electron transfer rates. A possible explanation for this observation is that it reflects an uneven surface distribution of immobilized duplexes. Duplexes in more crowded regions would experience a higher local concentration of negative charge, which would facilitate ferrocene oxidation and thus decrease E_0. At the same time, electroactivity from such more crowded duplexes would be expected to contribute more at lower sampling frequencies, where hindrance to rotational diffusion from the increased crowding should have less of an impact.

3.4. Nonfaradaic Surface Impedance (*Z*). Calculation of the impedance *Z* was performed on portions of ACV traces negative of the FcCA redox peak so as to extract information independent of tag electroactivity. *Z* therefore primarily represents charging/discharging of the duplex-modified electrode in response to the sinusoidal potential, and is expected to be sensitive to factors such as blockage of ion flow to the electrode and changes in polarizability and/or ionic concentrations in the near vicinity (i.e. within reach of surface fields) of the solid support. Thus, *Z* would be expected to be sensitive to nonspecific adsorption of protein to the MCH passivation layer, while specifically-bound protein may exert a weaker effect due to a spatial displacement of five nucleotides between the operator sites and the solid support (Table 1). Indeed, a key motivation for monitoring *Z* was to determine whether it may resolve nonspecific protein adsorption to MCH from specific DNA/protein interactions.

For the nonfaradaic conditions of measurement, the impedance can be approximately considered as that of an equivalent circuit of a resistance R in series with an interfacial capacitance C; in this basic model, $Z' = R$ and $Z'' = -1/(2\pi fC)$. C is a measure of the amount of charge that can be placed on the electrode before a certain potential difference is reached relative to solution; thus, changes that lower ability to screen electric fields at the electrode will lower C. Returning to Figure 4, at the lower frequency of 50 Hz where impedance was more capacitive, the increase in Z and $-\theta$ with Cro concentration is consistent with a decrease in C due to accumulation of material on the electrodes; e.g. due to replacement of higher permittivity water by lower permittivity protein. This trend is opposite to what would be expected for desorption of passivants, such as MCH.[48] At the higher frequency of 750 Hz additional features, traceable to variations in raw Z' data, appeared around C_P values consistent with onset of specific binding; however, both specific and nonspecific duplexes exhibited the same trends and thus attribution of these trends is uncertain. The similar responses for specific and nonspecific duplexes support the conclusion that impedance was primarily sensitive to nonspecific adsorption, independent of duplex sequence. Such behavior would be expected for direct adsorption of Cro to the MCH-passivated support.

4. Conclusions. Multimodal, multiplexed electrochemical analysis of DNA/protein interactions was implemented in the context of a model dimeric transcription factor, the bacteriophage λ Cro protein. Three different modalities, derived from a single electrochemical measurement, were compared for characterizing the binding of unlabeled protein to monolayers of immobilized, duplex DNA operators. Two of these modalities, the first based on monitoring the duplex rotational diffusive motions and the second on determining shifts in redox potential E_0 of

ferrocene moieties conjugated near the operator sites, provided clear signatures of specific binding. The third modality, which tracked changes in nonfaradaic impedance, proved insensitive to sequence-specific binding of Cro and instead was consistent with tracking of nonspecific adsorption to the solid support. These results support an overall picture in which, as protein concentration increases, specific docking of Cro with DNA operators is accompanied by gradual accumulation of nonspecifically associated protein on the electrode.

The primary advantage of E_0 relative to monitoring DNA diffusive motions for analyzing DNA/protein associations is that it does not rely on changes in signal amplitude, but rather tracks a peak position defined by energetics of tag oxidation. E_0 thus exhibits immunity to signal losses due to duplex desorption, tag degradation, or some other process. On the downside, E_0 was less effective in resolving specific from nonspecific interactions with λ Cro. Studies with additional proteins and various tag configurations would be needed to decide generality of these conclusions; regardless, the most versatile approach would be to implement these modalities in tandem. Lastly, by providing information on direct protein adsorption to the solid support, nonfaradaic impedance could serve as a control for interference from surface fouling.

Label-free methods for analysis of DNA/protein interactions would ideally be capable of tracking cooperative binding involving multiple operators and/or sequential assembly of protein subunits, whereby binding of an initial protein entity to DNA participates in guiding the binding of subsequent ones. λ Cro participates in such more complex interactions[26] and could serve in future studies to consider cooperativity of binding between multiple operators. Second, on the premise that shifts in tag redox potentials induced by protein binding provide a general detection strategy, further development through optimizing placement of electroactive tags and/or engineering their interaction with bound proteins is suggested. Third, further insight is needed

into the optimal interfacial design for quantitative, multiplexed assessment of DNA/protein interactions. Some of the interrelated questions of interest include how the distance of an operator site from the solid support, or the orientation of DNA immobilization, affect binding affinity, whether and how surface electric fields influence adsorption of proteins into DNA monolayers, and whether deliberate control through such fields could be used to enhance the ratio of specifically to nonspecifically bound protein.

Acknowledgements

This work was supported by the National Science Foundation under awards no. DGE-07-41714 and DMR 12-06754, and by the Polytechnic Institute of New York University.

References

1. P. Collas, *Mol Biotechnol*, 2010, **45**, 87–100.
2. S. Buratowski and L. Chodosh, *Curr. Protoc. Mol. Biol.*, 2001, **36**, 12.2.1–12.2.11.
3. A. J. Bonham, K. Hsieh, B. S. Ferguson, A. Vallee-Belisle, F. Ricci, H. T. Soh, and K. W. Plaxco, *J Am Chem Soc*, 2012, **134**, 3346–3348.
4. A. J. Bonham, T. Neumann, M. Tirrell, and N. O. Reich, *Nucl Acids Res*, 2009, **37**, e94.
5. M. L. Bulyk, *Adv Biochem Eng Biotechnol*, 2007, **104**, 65–85.
6. S. Mukherjee, M. F. Berger, G. Jona, X. S. Wang, D. Muzzey, M. Snyder, R. A. Young, and M. L. Bulyk, *Nat. Genet.*, 2004, **36**, 1331–1339.
7. A. K. Boal, E. Yavin, O. A. Lukianova, V. L. O'Shea, S. S. David, and J. K. Barton, *Biochemistry (Mosc.)*, 2005, **44**, 8397–8407.
8. E. M. Boon, A. L. Livingston, N. H. Chmiel, S. S. David, and J. K. Barton, *Proc Natl Acad Sci USA*, 2003, **100**, 12543–12547.
9. E. M. Boon, J. E. Salas, and J. K. Barton, *Nat Biotechnol*, 2002, **20**, 282–286.
10. Y. Wang, L. Guo, I. Golding, E. C. Cox, and N. P. Ong, *Biophys J*, 2009, **96**, 609–620.
11. A. A. Gorodetsky, A. K. Boal, and J. K. Barton, *J Am Chem Soc*, 2006, **128**, 12082–12083.
12. A. A. Gorodetsky, A. Ebrahim, and J. K. Barton, *J Am Chem Soc*, 2008, **130**, 2924–2925.
13. J. S. Shumaker-Parry, R. Aebersold, and C. T. Campbell, *Anal Chem*, 2004, **76**, 2071–2082.
14. E. A. Smith, M. G. Erickson, A. T. Ulijasz, B. Weisblum, and R. M. Corn, *Langmuir*, 2003, **19**, 1486–1492.
15. H. F. Teh, W. Y. X. Peh, X. Su, and J. S. Thomsen, *Biochemistry (Mosc.)*, 2007, **46**, 2127–2135.

16. F. Ricci, A. J. Bonham, A. C. Mason, N. O. Reich, and K. W. Plaxco, *Anal. Chem.*, 2009, **81**, 1608–1614.
17. R. J. White, N. Phares, A. A. Lubin, Y. Xiao, and K. W. Plaxco, *Langmuir*, 2008, **24**, 10513–10518.
18. Y. Xiao, T. Uzawa, R. J. White, D. Demartini, and K. W. Plaxco, *Electroanalysis*, 2009, **21**, 1267–1271.
19. A. Anne and C. Demaille, *J. Am. Chem. Soc.*, 2006, **128**, 542–557.
20. R. J. White and K. W. Plaxco, *Anal Chem*, 2010, **82**, 73–76.
21. F. G. Donnan, *J Membr Sci*, 1995, **100**, 45–55.
22. K. Wang, R. A. Zangmeister, and R. Levicky, *J Am Chem Soc*, 2009, **131**, 318–326.
23. H. Echols, *Ann Rev Genet*, 1972, **6**, 157–190.
24. M. Ptashne, *A Genetic Switch - Phage Lambda Revisited*, Cold Spring Harbor Laboratory Press, Cold Spring Harbor, NY, 3rd edn., 2004.
25. Y. Takeda, A. Folkmanis, and H. Echols, *J Biol Chem*, 1977, **252**, 6177–6183.
26. P. J. Darling, J. M. Holt, and G. K. Ackers, *J Mol Biol*, 2000, **302**, 625–638.
27. A. D. Johnson, B. J. Meyer, and M. Ptashne, *Proc Natl Acad Sci USA*, 1979, **76**, 5061–5065.
28. B. M. Hall, S. A. Roberts, A. Heroux, and M. H. Cordes, *J Mol Biol*, 2008, **375**, 802–811.
29. M. M. Bradford, *Anal Biochem*, 1976, **72**, 248–254.
30. S. J. Compton and C. G. Jones, *Anal Biochem*, 1985, **151**, 369–374.
31. D. Ge and R. Levicky, *Chem Commun*, 2010, **46**, 7190–7192.
32. U. Oesch and J. Janata, *Electrochim Acta*, 1983, **28**, 1237–1246.
33. G. Shen, N. Tercero, M. A. Gaspar, B. Varughese, K. Shepard, and R. Levicky, *J Am Chem Soc*, 2006, **128**, 8427–8433.
34. T. M. Herne and M. J. Tarlov, *J Am Chem Soc*, 1997, **119**, 8916–8920.
35. R. Levicky, T. M. Herne, M. J. Tarlov, and S. K. Satija, *J Am Chem Soc*, 1998, **120**, 9787–9792.
36. A. Bogomolova, E. Komarova, K. Reber, T. Gerasimov, O. Yavuz, S. Bhatt, and M. Aldissi, *Anal Chem*, 2009, **81**, 3944–3949.
37. R. E. Holmlin, X. Chen, R. G. Chapman, S. Takayama, and G. M. Whitesides, *Langmuir*, 2001, **17**, 2841–2850.
38. U. Rant, K. Arinaga, S. Fujita, N. Yokoyama, G. Abstreiter, and M. Tornow, *Nano Lett*, 2004, **4**, 2441–2445.
39. U. Rant, K. Arinaga, S. Fujita, N. Yokoyama, G. Abstreiter, and M. Tornow, *Langmuir*, 2004, **20**, 10086–10092.
40. S. D. O'Connor, G. T. Olsen, and S. E. Creager, *J Electroanal Chem*, 1999, **466**, 197–202.
41. D. D. Popenoe, R. S. Deinhammer, and M. D. Porter, *Langmuir*, 1992, **8**, 2521–2530.
42. R. Prins, A. R. Korswagen, and A. G. T. G. Kortbeek, *J Organomet Chem*, 1972, **39**, 335–344.
43. J. Holecek, K. Handlir, J. Klikorka, and N. D. Bang, *Collect. Czechoslov Chem Commun*, 1979, **44**, 1379–1387.
44. P. J. Darling, J. M. Holt, and G. K. Ackers, *Biochemistry (Mosc.)*, 2000, **39**, 11500–11507.
45. A. Anne and C. Demaille, *J. Am. Chem. Soc.*, 2008, **130**, 9812–9823.
46. W. Eimer and R. Pecora, *J Chem Phys*, 1991, **94**, 2324–2329.
47. H. H. Strey, V. A. Parsegian, and R. Podgornik, *Phys Rev Lett*, 1997, **78**, 895–898.
48. N. Tercero, K. Wang, and R. Levicky, *Langmuir*, 2010, **26**, 14351–14358.